Check for updates

ADVANCED MATERIALS TECHNOLOGIES
www.advmattechnol.de

A Mobile Two-Dimensional Ultrasound Focusing System for Personalized Healthcare Applications through a Dodecagonal Quasicrystal Patterned Planar Lens

*Yongrok Jeong, Hyeokjung Kang, Moonjeong Bok, Soon Hyoung Hwang, Sohee Jeon, Junseong Ahn, Ji-Hwan Ha, Jiwoo Ko, Jeong Won Park, Wonjae Choi, Inkyu Park, Namkyoo Park, and Jun-ho Jeong**

Ultrasound technology is widely utilized in applications, including tumor treatments, drug delivery, and skin care. However, improvements are required to prevent unwanted damage to non-targeted tissues. The ultrasound focusing technology, represented by the highly intensive focused ultrasound (HIFU) technology, is actively researched to handle this problem. However, current technology is primarily limited in the point focusing of the ultrasound. Some applications, such as drug delivery and skin care, require 2D-focusing of the ultrasound for effective utilization. Based on this necessity, this research proposes the rationally designed dodecagonal quasicrystal patterned (DQP) planar lens, which enables ultrasound focusing in 2D. The custom-built ultrasound scanning setup confirms the 2D focusing behavior of the DQP lens. Furthermore, the developed DQP lens is integrated into the mobile ultrasound 2D focusing (MU2F) system and solved the bulkiness limitation of the HIFU system. The proposed MU2F system is applied in microneedle-mediated drug delivery. The dramatic enhancement in the dissolution efficiency of the drug-containing microneedle (≈2.5×) compared with the case without the MU2F system is confirmed. Through the proposed MU2F system, ultrasound-based medical devices may widen their approachability from the clinic to the home.

1. Introduction

Ultrasound therapy is one of the most widely used medical techniques in tumor treatment,[1–3] pain relief,[4] drug delivery,[2,5–7] and skin care.[8–11] The therapy is conducted by applying high-intensity ultrasound to the demanding regions. However, since every noninvasive ultrasound use starts transmission at the skin's surface, harmful effects (e.g., histologic damage) are frequent to the normal tissue in the trajectory of the ultrasound.[12,13] Thus, to decrease these harmful effects, high-intensity focused ultrasound (HIFU) technology has been actively developed to focus the ultrasound at the target depth.[1,2,14,15] Two methods have embodied HIFU, the first is by including a concave morphology that can focus the ultrasound (e.g., self-focusing ultrasound, attachment of an additional lens), and the second is by arraying multiple ultrasound transducers

Y. Jeong, M. Bok, S. H. Hwang, S. Jeon, J. Ahn, J.-H. Ha, J.-ho Jeong
Department of Nano-manufacturing Technology
Korea Institute of Machinery and Materials
156, Gajeongbuk-ro, Yuseong-gu, Daejeon 34103, Republic of Korea
E-mail: jhjeong@kimm.re.kr

Y. Jeong, J. Ahn, J.-H. Ha, J. W. Park, I. Park
Department of Mechanical Engineering
Korea Advanced Institute of Science and Technology
291, Daehak-ro, Yuseong-gu, Daejeon 34141, Republic of Korea

H. Kang, N. Park
Department of Electrical and Computer Engineering
Seoul National University
Seoul 08826, Republic of Korea

J. Ko
Department of Materials Science and Engineering
Korea Advanced Institute of Science and Technology
291, Daehak-ro, Yuseong-gu, Daejeon 34141, Republic of Korea

J. W. Park, W. Choi
Interdisciplinary Materials Measurement Institute
Korea Research Institute of Standards and Science
267, Gajeong-ro, Yuseong-gu, Daejeon 34113, Republic of Korea

The ORCID identification number(s) for the author(s) of this article can be found under https://doi.org/10.1002/admt.202202173

© 2023 The Authors. Advanced Materials Technologies published by Wiley-VCH GmbH. This is an open access article under the terms of the Creative Commons Attribution-NonCommercial License, which permits use, distribution and reproduction in any medium, provided the original work is properly cited and is not used for commercial purposes.

DOI: 10.1002/admt.202202173

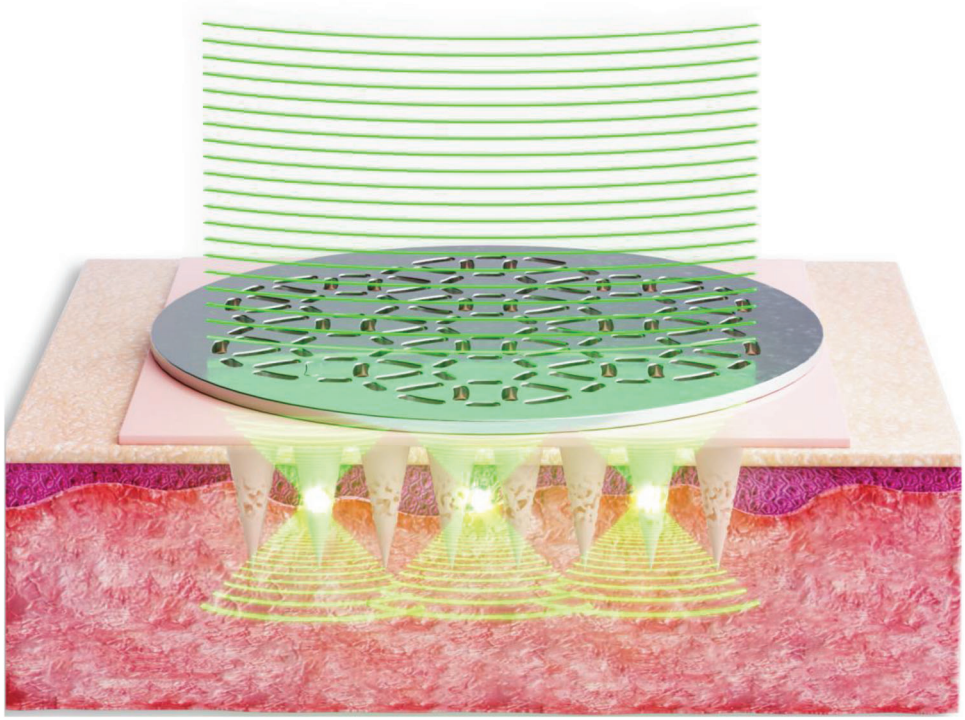


Figure 1. The mobile ultrasound 2D focusing system is based on the dodecagonal quasicrystal patterned (DQP) lens and mobile ultrasound transducer. Planar ultrasound wave propagates through the designed DQP lens and constructs a 2D focal plane at the microneedle. Focusing the ultrasound at the microneedle helps dissolve and activate the drug in the microneedle. This device has been applied in the drug-delivery system.

and focusing its shot angle.[16–18] Although the device is advantageous in personal healthcare, mobile use is limited due to the system's intrinsic bulkiness. This bulkiness restricts the approachability of the HIFU system, at least on the scale of local clinics or laboratories. Thus, the current HIFU system is unlikely to be used in an individual's life, although the technology is promising. Furthermore, the current HIFU aims to focus all the power on a single point. However, some applications, such as drug delivery or skin care, require focus on the ultrasound at the plane, not the point.

This study developed the mobile ultrasound 2D focusing (MU2F) system by adopting a dodecagonal quasicrystal patterned (DQP) planar lens with a small thickness (0.3 mm). The dodecagonal quasicrystal pattern was selected to maximize the fill ratio of the ultrasound focusing pattern. In addition, the appropriate ratio between the pitch and radius of the pattern was selected to maximize the effective area of the focusing plane. The 2D ultrasound focusing through the DQP lens was confirmed and compared with the simulation results via a custom-built ultrasound scanning setup. Additionally, the DQP lens with the selected pattern was integrated into the MU2F system and applied to the drug delivery system via a microneedle patch (**Figure 1**).

2. Results and Discussion

2.1. Design of the Dodecagonal Quasicrystal Patterned Lens

Typically, to reduce the volume of the HIFU system, meta-lens technology is used in two directions: space coiling meta-lens[19,20] and planar meta-lens.[21] Between them, planar meta-lens has been widely applied due to their facile fabrication method, but the previous meta-lens system was still limited in the number of foci: the acoustic wave can only be focused at a single point. However, the main reason for the ultrasound focusing in the HIFU system is not by single-point focusing but by lowering the ultrasound intensity in the non-target regions. Thus, in the case of applications that require ultrasound to be applied to a wide area, such as drug delivery and skin care, the HIFU system's effectiveness may be inhibited by their single-point ultrasound focusing. In a similar principle to the planar meta-lens (interference between diffracted waves), this study proposes the DQP planar lens, which inherits the advantages of the planar meta-lens, including reduced bulkiness and an ultrasound concentrating feature. In contrast, the ultrasound's focus is not restricted to a single point but to the plane.

The ultrasound's characteristics were studied for the lens design. The ultrasound generated from the transducer can be divided into two stages: near-field wave and far-field wave. In the case of a near-field wave, due to the short distance between the wavefront and transducer, the wave should be approximated as a non-stabilized, spherical, or parabolic wave.[22] On the other hand, the far-field wave can be treated as a stabilized planar wave and thus has been adopted for this research. The distance to the boundary of near-field and far-field waves from the transducer (N) can be calculated by[22]:

$$N = \frac{D^2}{4\lambda} = \frac{D^2 f}{4c} \tag{1}$$

© 2023 The Authors. Advanced Materials Technologies published by Wiley-VCH GmbH

2365709x, 2023, 16, Downloaded from https://onlinelibrary.wiley.com/doi/10.1002/admt.202202173 by South Korea National Provision, Wiley Online Library on [11/09/2023]. See the Terms and Conditions (https://onlinelibrary.wiley.com/terms-and-conditions) on Wiley Online Library for rules of use; OA articles are governed by the applicable Creative Commons License

2365709x, 2023, 16, Downloaded from https://onlinelibrary.wiley.com/doi/10.1002/admt.202202173 by South Korea National Provision, Wiley Online Library on [11/09/2023]. See the Terms and Conditions (https://onlinelibrary.wiley.com/terms-and-conditions) on Wiley Online Library for rules of use; OA articles are governed by the applicable Creative Commons License

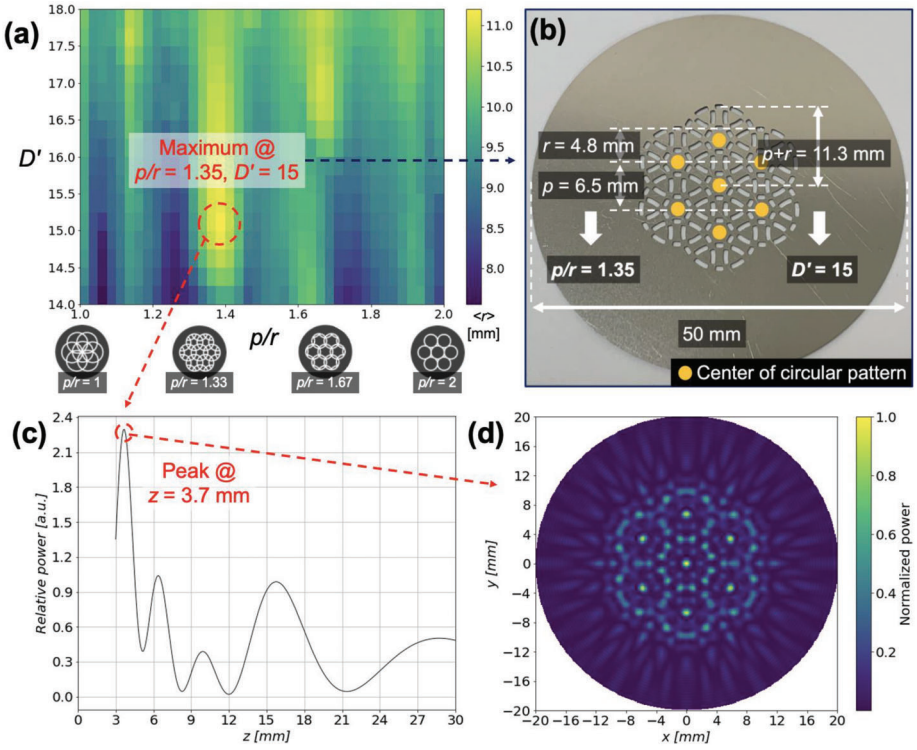


Figure 2. The design process for the dodecagonal quasicrystal patterned (DQP) lens. a) The various p/r and D' values for the DQP lens. The design that maximizes the power-weighted radius <r> was selected. Therefore, $p/r = 1.35$ and $D' = 15$ were adopted to be used further. b) The DQP lens was fabricated to follow the predefined p/r and D'. c) At the selected design point, the power was focused at $z = 3.7$ mm, with a ratio of ≈2.3×, compared to the incident ultrasound's power. d) The simulated power distribution of the propagated ultrasound at peak point ($z = 3.7$ mm).

where D (m) is the diameter of the ultrasound transducer, f (Hz) is the frequency of the generated ultrasound, c (m s^{-1}) is the velocity of sound in the target medium, and λ (m) is the wavelength of the ultrasound. This research used the ultrasound transducer of $D = 25$ mm and $f = 1$ MHz in water ($c = 1498$ m s^{-1}). Thus, N can be calculated as 10.4 cm. Therefore, the planar wave was used as the type of the ultrasound source for the simulation, and the DQP lens was placed 11 cm (>10.4 cm) from the ultrasound transducer.

The planar wave was propagated and diffracted by the DQP lens. A hexagonally-patterned circle, equivalent to the dodecagonal quasicrystal pattern, was adopted to maximize the fill ratio of the pattern that can be included in the diffraction. The dodecagonal quasicrystal pattern is a pattern that maximizes the fill ratio and forms a multifocal diffraction pattern, and similarly, it is used in this study as a multifocal acoustic wave filter with maximized fill ratio of the pattern.[23,24] Detailed dodecagonal quasicrystal patterns can be generated by determining three factors: the pitch between circles (p), the radius of the circle (r), and the thickness of the pattern (d). For further optimization, d was fixed as 0.6 mm.

Based on these design parameters, the calculation was conducted by Rayleigh–Sommerfeld diffraction integral. From this method, the propagated energy $U(x, y, z)$ can be calculated by[25]

$$U(x,y,z) = \frac{1}{i\lambda}\iint U(x',y',0)\frac{ze^{ikR}}{R}\mathrm{d}x'\mathrm{d}y' \quad (2)$$

where λ is the wavelength of the propagated waves, $k = \frac{2\pi}{\lambda}$ is the propagation constant, (x, y, z) is the point placed at the plane of interest, $(x', y', 0)$ is the point placed at the plane of source, and $R = \sqrt{(x-x')^2 + (y-y')^2 + z^2}$, with coordinates shown in Figure S1, Supporting Information. Since this calculation is used to decide the details of the dodecagonal quasicrystal pattern that maximizes the ultrasound focusing area, a power-weighted radius <r> was adopted for optimization. <r> can be calculated by

$$\langle r \rangle = \frac{\int rP(x,y)\,\mathrm{d}S}{\int P(x,y)\,\mathrm{d}S} \quad (3)$$

where $P(x, y)$ denotes the power at the point (x, y) and $r = \sqrt{x^2 + y^2}$. This factor can be used as the indicator for the power-focused plane size. Thus, this factor is maximized via simulation. Two factors were selected to be optimized: $\frac{p}{r}$ and $D' = \frac{2(p+r)}{\lambda}$. By determining these factors, the morphology of the DQP lens can be settled. For various p/r and D', the corresponding <r> was calculated with sweeping z. The maximum value of <r> for each sweeping under various conditions is visualized in **Figure 2**a. As a result, the propagated energy can be focused on the plane with maximized <r> at $p/r = 1.35$ and $D' = 15$. The corresponding morphology of the DQP lens can be found in Figure 2b. For the selected design, the specifications were simulated, as shown in Figure 2c,d. Figure 2c shows the power of the propagated wave on the z-axis behind the DQP lens, and it was confirmed that ultrasound focusing was performed in a factor of about 2.3 at $z = 3.7$

© 2023 The Authors. Advanced Materials Technologies published by Wiley-VCH GmbH

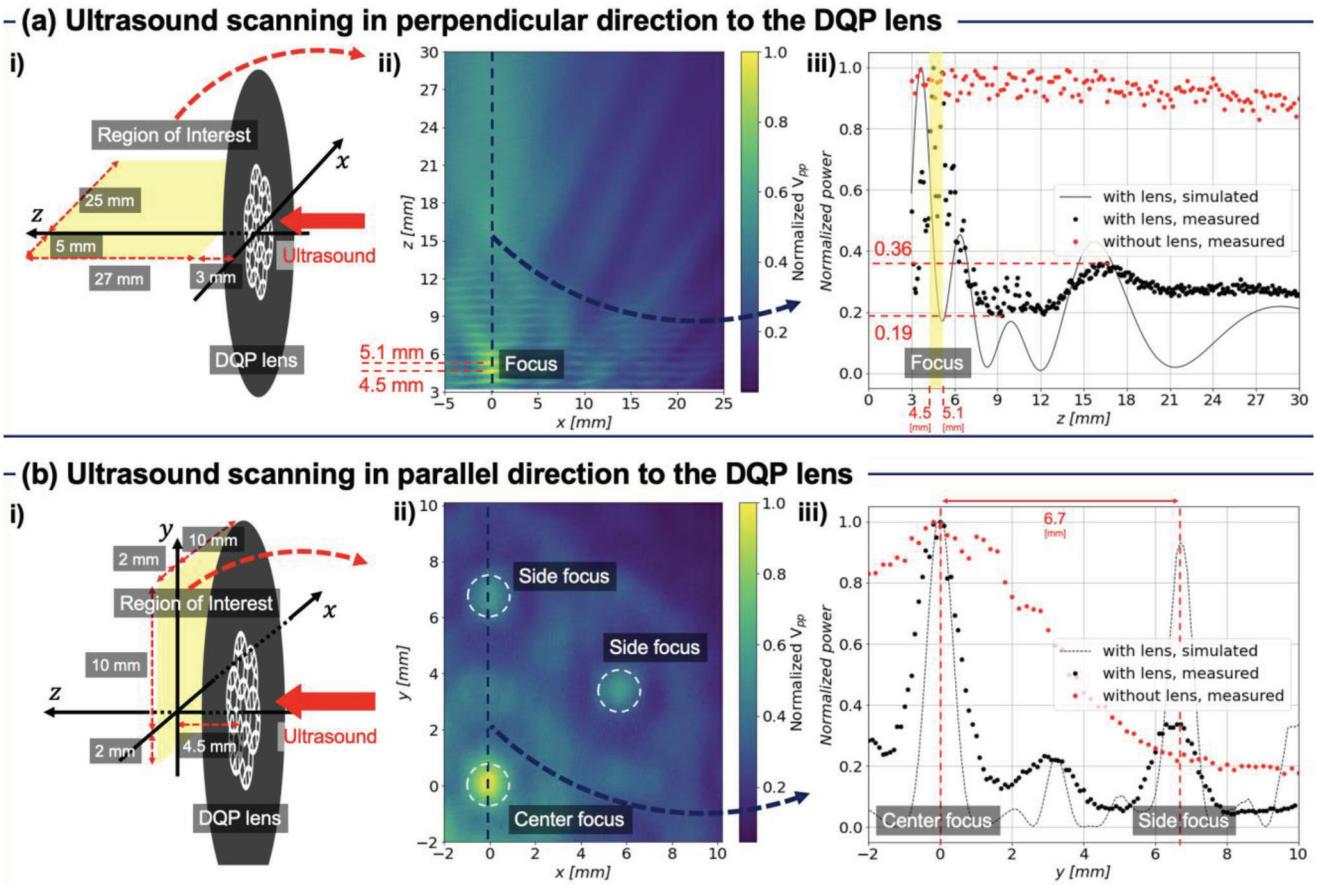


Figure 3. The dodecagonal quasicrystal patterned (DQP) planar lens results. 3D ultrasound scanning was conducted a) in a perpendicular direction to measure the focal depth of the DQP lens (z = 4.5–5.1 mm) and b) in a parallel direction to confirm the 2D focusing behavior of the DQP lens at the measured focal depth (z = 4.5 mm). The i) experimental condition, ii) 3D scanning results in the heatmap graph, and iii) scattering plot for the mainly monitored region from the heatmap graph and confirmation by the simulated result of the corresponding region are shown. Both results confirmed that the DQP lens results were similar to the simulated results: focal depth of 4.5–5.1 mm and plane-like multi-focal behavior with 6.7 mm between the individual focus points.

mm. Figure 2d shows the energy distribution at the focal plane (z = 3.7 mm) and the concentration of power at the center and borderline of the circle. The ultrasound focusing on the borderline of the circle can be activated via the dodecagonal quasicrystal pattern of the DQP lens. Thus, this pattern can maximize the 2D focusing of the ultrasound.

2.2. Demonstration of the Dodecagonal Quasicrystal Patterned Lens

First, ultrasound scanning was conducted perpendicularly with the DQP lens to confirm the depth of the focal plane. The scanning was conducted in the region of interest, as denoted in **Figure 3**a-i, and the result can be found in Figure 3a-ii. The initial position of the ultrasound receiver was set at z = 3 mm to avoid collision with the lens. This data confirmed the clear focusing of the ultrasound in the region of z = 4.5–5.1 mm. From the scanning data, the z-normalized power graph along the z-axis (blue dotted line in Figure 3a-ii) was depicted in Figure 3a-iii. Compared to the scanning results without the DQP lens (Figure S2, Supporting Information), it is confirmed that the focusing of the ultrasound is possible through the DQP lens. This graph concludes that the first valley beside the focus has 19% power, and the second peak has 36% power, regarding the power at focus. In other words, the power of the focus point was ≈5.3 times larger than the power of the first valley. The simulation result in Figure 2, where a similar tendency of the power concentration change was observed, supports this conclusion. For example, the z-value of the peak and valley are similar; the first valley of the measured data was observed at z at 10.5 mm, and the first valley of the simulated data was observed at z at 10 mm. However, blunting of the transmitted power was observed in the actual experiment compared to the simulation data. This blunting may be caused by two reasons; the first is that the ultrasound receiver reads the average power of the small area, not the point. Since the average power of the area was approximated as point power in the actual experiment, blunting of the power is possible. The second is the wave's propagation could have been affected due to the ultrasound receiver's movement, causing the wave-like pattern in Figure 3a-ii. As a result, the focusing of the ultrasound was enabled by the proposed DQP lens, and the focal depth was measured in the range of

© 2023 The Authors. Advanced Materials Technologies published by Wiley-VCH GmbH

2365709x, 2023, 16, Downloaded from https://onlinelibrary.wiley.com/doi/10.1002/admt.202202173 by South Korea National Provision, Wiley Online Library on [11/09/2023]. See the Terms and Conditions (https://onlinelibrary.wiley.com/terms-and-conditions) on Wiley Online Library for rules of use; OA articles are governed by the applicable Creative Commons License

4.5–5.1 mm, similar to the simulations. The difference between the experimental results and the simulation may be originated from 1) measurement error from ultrasound receiver (it measures the ultrasound intensity as a volume average rather than a point), and 2) error by the movement of ultrasound receiver that cause the movement of the medium.

Next, ultrasound scanning was conducted parallel to the DQP lens, and the z-axis position of the focus point was $z = 4.5$ mm to identify the 2D focusing behavior of the DQP lens. The scanning was conducted in the region of interest, as denoted in Figure 3b-i, and the results can be found in Figure 3b-ii. The focusing behavior of the scanning results at the plane is similar to the simulated results, with focus at the boundary and maximized focusing at the center of the circle. Furthermore, the y-normalized power graph along the y-axis (blue dotted line in Figure 3b-ii) was depicted in Figure 3b-iii. According to the simulation, the focusing power for the center and sides should be similar (about 93% for the center). However, the measured value shows less power (about 34% for the center) than the simulated result. The results measured without a lens (Figure S2, Supporting Information), where the power delivery by ultrasound transducer is low (<30% for the center) at the edge, confirms this phenomenon. Two reasons could cause this decrease; the first is the ultrasound source position may not be perfectly aligned. The second is the amount of the evanescence wave is possibly more significant than expected because the applied wavefront in this experiment was a quasi-planar wave, not the perfect planar wave used in the simulation.

2.3. Demonstration of the Mobile Ultrasound 2D Focusing System

The DQP lens-based MU2F system was designed (Figure S3a, Supporting Information) and fabricated (Figure S3b, Supporting Information) to build the far-field ultrasound propagation environment. An ultrasound stabilizer, with a length of 11 cm ($>N = 10.4$ cm), was inserted in front of the mobile ultrasound generator. The stabilizer transforms the non-stabilized ultrasound wave from the transducer to the far-field, planar ultrasound to be applied at the DQP lens. The stabilized planar ultrasound wave passes through the DQP lens and is focused on the designed focal plane. The end cap module fixed the DQP lens in front of the stabilizer to enable the facile replacement of various DQP lenses. The various lens designs depend on the area of the plane, which depends on the application target.

Since the proposed MU2F system was not waterproof, it was difficult to use the 3D ultrasound scanning setup to demonstrate the MU2F system. Instead, a resistance temperature detector (RTD) array film integrated with a gelatin bio-phantom was utilized to demonstrate the MU2F system. The RTD array was used to monitor the temperature change as focused ultrasound induces higher temperature increases than other regions since the focusing of the ultrasound denotes the focusing of the energy. For the RTD array, a serpentine-patterned electrode was adopted (Figure S4a,b, Supporting Information), and the temperature can be measured by

$$\frac{R - R_0}{R_0} = \frac{\Delta R}{R_0} = \alpha T[^\circ\mathrm{C}] + k \tag{4}$$

where T (°C) is the present temperature, R_0 (Ω) is the resistance of the RTD at 27 °C, R (Ω) is the resistance of the RTD at T, α ($^\circ\mathrm{C}^{-1}$) is the temperature coefficient of resistance of the RTD, and k is a constant.

As shown in **Figure 4**a, ultrasound was generated from the mobile transducer, stabilized by the ultrasound stabilizer, and focused on the gelatin bio-phantom by the DQP lens. When the setup was viewed from the wall side (Figure 4b), a 3 mm distance between the DQP lens and the region of interest was designed and measured; the thickness of the region of interest is 4 mm. Therefore, the energy distribution in the depth range of 3–7 mm from the DQP lens could be observed with this setup. Each sensor represents a specific focal depth, as shown in Figure 4c. Among them, the focal points of the DQP lens was placed between sensor #2 (depth of 6–6.5 mm) and sensor #6 (depth of 4–4.5 mm). Thus, in this research, sensors #2–#6 were mainly picked as regions of interest and monitored.

The temperature change of each sensor after the ultrasound appliance is shown in Figure 4d. Since the focal plane ($z = 4.5$–5.1 mm) was placed at the region of sensor #5 ($z = 4.5$–5.0 mm), the temperature change of sensor #5 was the most significant compared to the other sensors. Although the DQP lens enables the plane-like focusing of the ultrasound, it is not focused in a perfectly planar shape. Instead, the energy distribution spreads out from focus points. Therefore, the number of focus points captured by each sensor may affect the temperature change. In this point of view, even though sensor #2 contained two local focus points, the same as sensor #5, a clear difference in temperature change was shown between sensors #2 and #5. The difference may originate from whether the depth represented by each sensor contains the focal plane. From this result, the MU2F system, composed of a DQP lens and a mobile ultrasound device, was successfully demonstrated. The focus of the ultrasound was proven by monitoring the partial temperature changes of the human tissue-mimicked gelatin phantom.

2.4. Application of the Mobile Ultrasound 2D Focusing System in Drug Delivery

Although injections by a needle are the most widely used drug delivery method, it still has several shortcomings, such as patient fear, potential insertion injury, and contagions. Numerous drug delivery methods, mediated by microneedles, ultrasound, and iontophoresis, have been actively researched to solve these issues and replace injections by a needle.[7] Among them, microneedle-mediated and ultrasound-based drug delivery can be simultaneously used synergistically. When they are utilized simultaneously, the drug delivery via a microneedle patch can be enhanced by ultrasound. Even unintended damage in the non-targeted tissues can be prevented by applying the proposed MU2F system.

The microneedle adopted in this research was fabricated with a matrix material of salmon DNA and a rhodamine drug model. Details about the reason for the utilization of each material can be found in the previous paper,[7,26,27] and details about the fabrication of the microneedle patch can be found in the Experimental Section. As a result, the fabricated needle patch had a diameter of 5 mm and a needle length of 600 μm (**Figure 5**a). An in vitro drug delivery test with the fabricated microneedle and

© 2023 The Authors. Advanced Materials Technologies published by Wiley-VCH GmbH

2365709x, 2023, 16, Downloaded from https://onlinelibrary.wiley.com/doi/10.1002/admt.202202173 by South Korea National Provision, Wiley Online Library on [11/09/2023]. See the Terms and Conditions (https://onlinelibrary.wiley.com/terms-and-conditions) on Wiley Online Library for rules of use; OA articles are governed by the applicable Creative Commons License

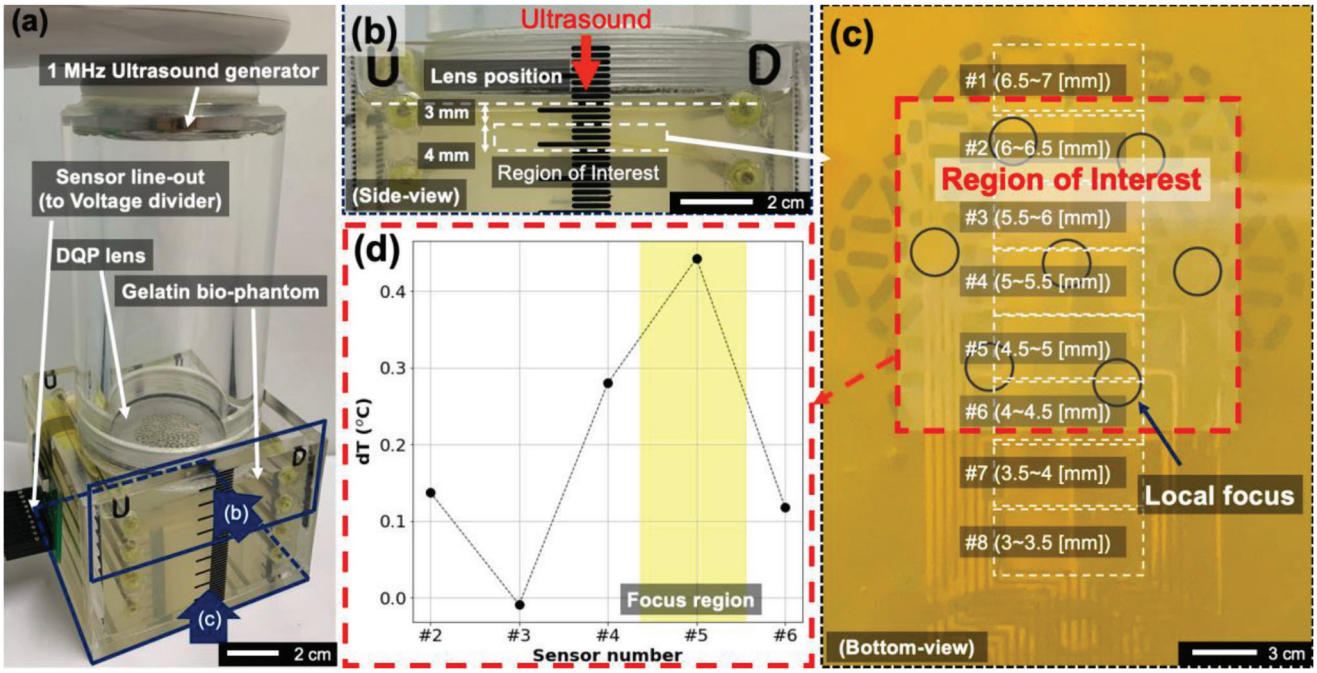


Figure 4. The mobile ultrasound 2D focusing (MU2F) system's results: a) The MU2F system was demonstrated by acquiring the energy density of the tissue-mimicked gelatin bio-phantom. A resistance temperature detector (RTD) array film was inserted into the gelatin phantom to investigate the energy density. b) From its side-view, it is confirmed that the RTD array monitors the energy density for a depth range of 3–7 mm from the dodecagonal quasicrystal patterned (DQP) lens. c) From its bottom view, it is confirmed that the DQP lens was included in the range of sensors #2–#6. Therefore, sensors #2–#6, which represent a depth of 4–6.5 mm, from the DQP lens, have been picked as the region of interest. d) The temperature change was monitored for each of the sensors. As a result, the increase in temperature was maximized at the focal plane of the DQP lens.

the human tissue-mimicked gelatin bio-phantom confirmed the enhancement of the drug delivery by the proposed MU2F system. Three groups were tested and analyzed: the control group (no ultrasound propagation), the non-focused group (ultrasound propagated but not focused at the microneedle), and the focused group (ultrasound propagated and focused on the microneedle). The distance from the DQP lens to the microneedle was controlled by replacing the end cap. In the non-focused experiment, an end cap with a 2 cm depth was used (Figure 5b-i), and in the focused experiment, an end cap with a 0.5 cm depth was used (Figure 5b-ii). The microneedle patch was first inserted into the gelatin bio-phantom, and the MU2F system was loaded upright onto the patch at the center of the DQP lens (Figure 5b-iii). For each group, the drug delivery efficiency (dissolution efficiency, ϵ) was calculated by dividing the transferred amount of rhodamine in the gelatin bio-phantom by the total amount of rhodamine inserted into the microneedle.

After 10 min of ultrasound propagation, the control, and the non-focused group had ϵ of 40%, while the focused group had ϵ of 98%, which is ≈2.5 times larger. These results lead to two conclusions; the first is that the non-focused group showed a minute difference in ϵ compared to the control group, which denotes that the effect of the ultrasound at the out-of-focal plane is minute, thereby safe for the non-focused region. The second is that the proposed MU2F system can enhance the dissolution of the microneedle patch when they are focused.

Previous research shows that the dissolution of the microneedle patch was active just after the penetration of the microneedle. Still, it is decelerated when the adjacent tissues are saturated with the target drug.[7,26,27] Therefore, the change in ϵ for the control and non-focused group is small for the first 10 min of the ultrasound propagation. However, utilization of the MU2F system accelerated the dissipation of the dissolved and saturated drug to the adjacent tissue. Thereby the delivery of the drug inside the microneedle was accelerated. By comparing the results of the non-focused and focused groups, it can be confirmed that the proposed MU2F system enabled this phenomenon.

3. Conclusion

Ultrasound technology has been widely utilized in applications, including tumor treatments, drug delivery, and skin care. Thus, the importance of ultrasound technology is expanding. HIFU technology, which enables the focusing of the ultrasound at the target region, has been actively researched for safer use. This technology usually targets the 1D-focusing of the ultrasound to maximize the intensity. However, some applications, such as drug delivery and skin care, require 2D-focusing of the ultrasound instead of 1D-focusing. Due to this necessity, this research designed, fabricated, and confirmed the DQP planar lens, which enables the 2D-focusing of the ultrasound. Furthermore, the developed DQP lens was integrated into the MU2F system to solve the bulkiness issue of the HIFU system. Application of the MU2F system to microneedle-mediated drug delivery dramatically enhanced the dissolution efficiency of the microneedle (about 2.5×) compared to without the MU2F system. Although the HIFU system has only been used for medical purposes, the developed MU2F system could potentially widen the HIFU system's

© 2023 The Authors. Advanced Materials Technologies published by Wiley-VCH GmbH

2365709x, 2023, 16, Downloaded from https://onlinelibrary.wiley.com/doi/10.1002/admt.202202173 by South Korea National Provision, Wiley Online Library on [11/09/2023]. See the Terms and Conditions (https://onlinelibrary.wiley.com/terms-and-conditions) on Wiley Online Library for rules of use; OA articles are governed by the applicable Creative Commons License

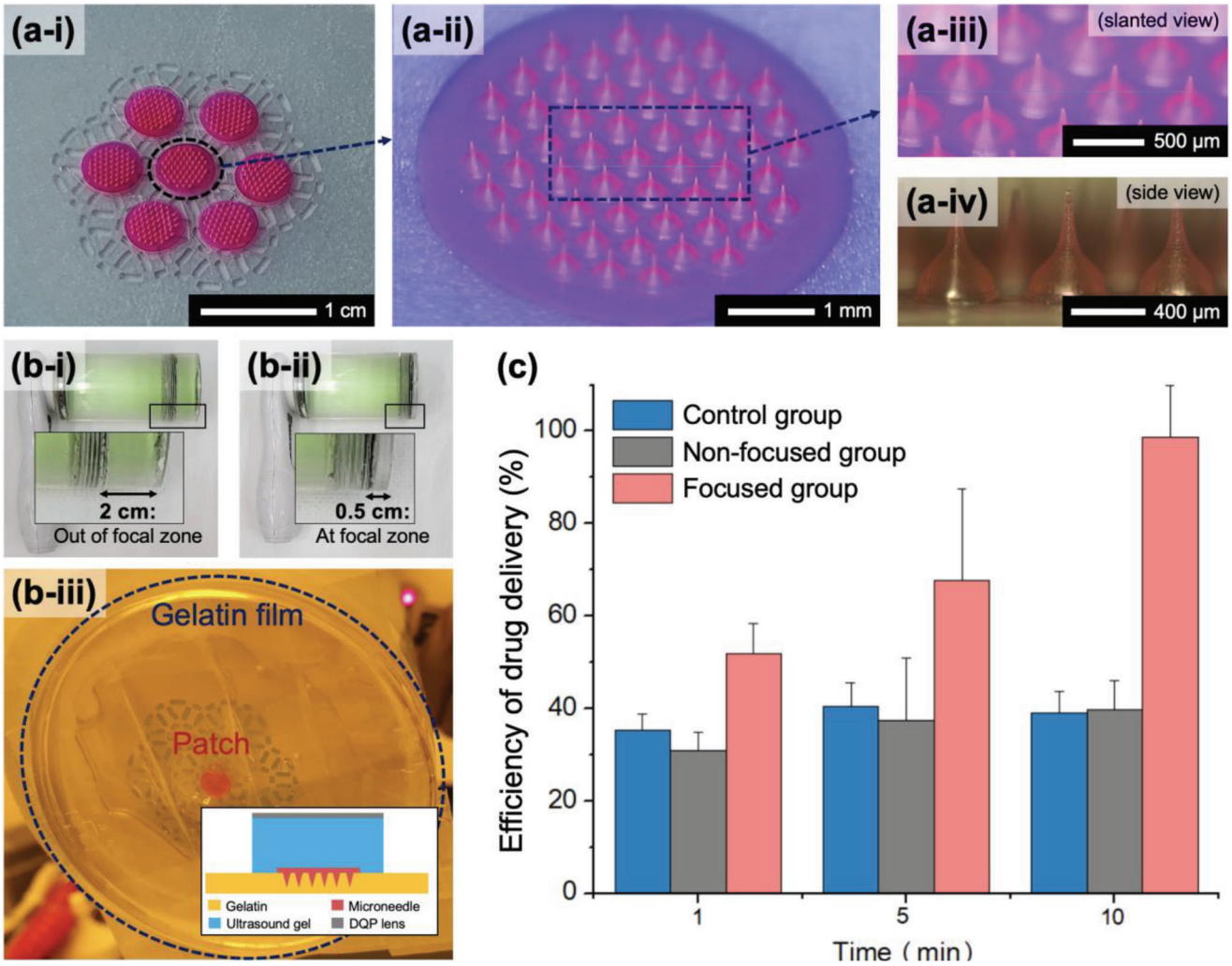


Figure 5. The mobile ultrasound 2D focusing (MU2F) system applied in microneedle-mediated drug delivery. a) A microneedle patch was fabricated with a 5 mm diameter and a hexagonal array pattern. b) Controlling the focal depth of the MU2F system by replacing the end cap. i) The non-focused group is where the ultrasound was focused before reaching the skin, and ii) the focused group is where the ultrasound was focused at the microneedle. iii) The system on which the experiment was performed. c) The experimental results for the three groups. The focused group represents the simultaneous usage of microneedle-mediated drug delivery and ultrasound-based assistance in drug delivery. Further, it is the only group that showed high drug delivery efficiency.

applications due to the ultrasound's focusing region (1D → 2D) and the HIFU system's approachability (from clinic to home).

4. Experimental Section

Design of the Dodecagonal Quasicrystal Patterned Lens: Based on the governing equation (Section 2.1), numerical simulation by MATLAB was used for the design and optimization of the DQP lens.

Fabrication and Demonstration of the Dodecagonal Quasicrystal Patterned Lens: The designed DQP lens was fabricated by the conventional silkscreen metal mask fabrication method (SUS; $t = 0.3$ mm). The fabricated DQP lens was installed in a custom-built ultrasound 3D scanning setup (Figure S5a, Supporting Information) and tested. The custom-built ultrasound 3D scanning setup was composed of the 3D-movable stage combined with the end effector of the ultrasound receiving system (ETA-100L Ultra; Xarion, Austria) and ultrasound generating system, which comprised the function generator (33550B; Keysight, USA), the amplifier (HAS 4052; NF, Japan), and the ultrasound transducer (V302-SU; Olympus, Japan) in the fixed site. Furthermore, 11 cm of distance between the generator and the DQP lens was set to obtain far-field ultrasound. Because of the ultrasound receiver's volume, 3 mm of the distance between the DQP lens and the origin point of the ultrasound receiver was set. In addition, the moving speed of the ultrasound transducer was set at 1 mm s^{-1}. The detailed scanning direction of experiments in Figure 3 can be found in Figure S5b,c, Supporting Information. The scanning results were used to calculate the peak-to-peak voltage value (V_{pp}) from the maximum and minimum voltage obtained. With the calculated V_{pp} for each point, a 2D heatmap was drawn, and for specific regions, a 2D scatter plot was drawn by Python's "matplotlib" library. For the 2D scatter plot drawing, the normalized power was calculated by the square of the V_{pp} and normalized by its maximum value.

Fabrication of the Dodecagonal Quasicrystal Patterned Lens Module: The LW-009 hand-held ultrasound instrument (Continuous, 1 MHz frequency; Beemyi, China) was used as the mobile ultrasound source device. In addition, the abovementioned custom-built 3D ultrasound scanning setup

© 2023 The Authors. Advanced Materials Technologies published by Wiley-VCH GmbH

2365709x, 2023, 16, Downloaded from https://onlinelibrary.wiley.com/doi/10.1002/admt.202202173 by South Korea National Provision, Wiley Online Library on [11/09/2023]. See the Terms and Conditions (https://onlinelibrary.wiley.com/terms-and-conditions) on Wiley Online Library for rules of use; OA articles are governed by the applicable Creative Commons License

checked the device's performance. The frequency of the generated ultrasound was calculated via the fast Fourier transform method and measured at ≈1 MHz, the same as the specification (Figure S6, Supporting Information). In front of the LW-009, a custom-built ultrasound stabilizer made with acryl was attached by epoxy glue, and an end cap part made with acryl was attached with a screw. The DQP lens was inserted with O-ring sealing between the stabilizer and the end cap to prevent ultrasound gel leakage. Ultrasound gel, without bubbles, filled the stabilizer (Eco gel 99; Seung won medical corp., Korea) for the transfer of ultrasound.

Demonstration of the Dodecagonal Quasicrystal Patterned Lens Module: The RTD sensor array was fabricated and calibrated before assembling the RTD sensor array and gelatin phantom (Figure S4a,b, Supporting Information). For the electrode material of RTD, gold (Au) was used due to its stability in a chemically-active/high-temperature environment and enough temperature coefficient of resistance. Conventional electron beam deposition and lift-off methods were used to pattern the Au film. More details about RTD fabrication can be found in the previous paper.[28] For the RTD calibration, the fabricated RTD film and two reference temperature sensors (midi LOGGER GL220; Graphtec Corporation, Japan, was used as data logger, and ST-50; RKC Instruments, Japan, was used as a temperature sensor) were attached to the silicon wafer that was utilized as a temperature equalizer (Figure S4c, Supporting Information). The average value of the two reference temperature sensors was used for the reference temperature. A voltage divider (Figure S4d, Supporting Information) and a LabView-based voltage readout system (USB 6211; National Instruments, USA) were used to measure the resistance of the RTD sensor. The measured resistance value was calibrated based on the reference temperature, following Equation (4). Detailed calibration results of the RTD can be found in Figure S4e and Table S1, Supporting Information.

A fabricated sensor was attached to the rods of the custom-built gelatin chamber. First, the gelatin solution was prepared by dissolving gelatin powder (300 g Bloom, Type A; Sigma-Aldrich, USA) in 10% w/w deionized water by mixing with magnetic stirring at 500 rpm at 65°C for 5 h. The dissolved gelatin solution was poured into the chamber until the surface of the gelatin touched the top point of the highest rod. Next, the chamber was cooled to room temperature (27 °C) to coagulate the gelatin. On the RTD-integrated gelatin phantom, ultrasound gel was spread for seamless sealing between the MU2F system and the gelatin phantom. After setting, ultrasound was applied for 1 min. For each experiment, the maximum power of the LW-009 mobile ultrasound generator was used. The resistance for each RTD was measured before and after applying ultrasound, and the difference was calculated and analyzed (Figure 4).

Fabrication of the Salmon DNA-Based Microneedle: The 3D-printed master mold of the microneedle hexagonal array (600 μm height, 10 μm tip diameter, and 500 μm pitch) that was placed in the patch with a diameter of 5 mm was replicated by poly-dimethylsiloxane (PDMS; Sylgard 184, Dow corning, USA). PDMS was cured at 50 °C for 6 h with a mixing ratio of 10:1 between the matrix agent and the curing agent. The rhodamine B-DNA solution was prepared by dissolving 0.0075 g rhodamine B (>98% purity; Acros-Organics, Geel, Belgium) and 30 g of 3% w/w salmon DNA (highly polymerized deoxyribonucleotides, sodium salt, low M_w, medical grade, extracted from salmon milt, HTL Biotechnology, France) in deionized water. The rhodamine B-DNA solution (1.5 mL) was poured into the replicated mold, vacuumed for 5 min, and dried by natural convection for 12 h. After drying, taping detached the rhodamine-dyed DNA microneedle patch from the PDMS replicated mold.

Procedure for the Microneedle-Based Drug Delivery Experiment: The gelatin solution was poured into a 2″ petri dish until 5 mm thickness was reached. After pouring, the gelatin was cooled for coagulation. Over the coagulated gelatin, film coating by parafilm enabled the targeted dissolution of only the microneedle. The dissolution test was performed with and without the MU2F system for the targeted time. When the MU2F system was applied for the dissolution, the ultrasound gel was seamlessly applied between the system and the microneedle to avoid the unintended decaying of the ultrasound. After the target time, the microneedle patch was delaminated from the gelatin bio-phantom to stop the dissolution. The rhodamine inside the gelatin phantom was extracted by immersing the gelatin phantom into a bleaching solution (methanol:deionized water:acetic acid = 5:4:0.5) for 8 h. For comparison, the remainder of the microneedle was cut and immersed into a bleaching solution. The rhodamine concentration in the bleaching solution was calculated based on the Beer–Lambert law, with the absorbance obtained by ultraviolet–visible spectroscopy (Neosys-2000, Scinco, Korea). For accuracy, the experiments were repeated three times ($n = 3$), and the standard deviation from each result is denoted in Figure 5c.

Supporting Information

Supporting Information is available from the Wiley Online Library or from the author.

Acknowledgements

Y.J., H.K., and M.B. equally contributed to this work. This research was supported by the Center for Advanced Meta-Materials (CAMM) funded by the Ministry of Science, ICT and Future Planning as Global Frontier Project (CAMM No. 2014M3A6B3063707). N.P. acknowledges support from National Research Foundation of Korea (NRF) through the Global Frontier Program (no. 2014M3A6B3063708). H.K. acknowledges the Hyundai Motor Chung Mong-Koo fellowships.

Conflict of Interest

The authors declare no conflict of interest.

Data Availability Statement

The data that support the findings of this study are available from the corresponding author upon reasonable request.

Keywords

acoustic lens, dodecagonal quasicrystals, drug delivery, microneedles, planar lens

Received: December 22, 2022
Revised: May 14, 2023
Published online: July 3, 2023

[1] Y.-F. Zhou, *World. J. Clin. Oncol.* **2011**, *2*, 8.
[2] X. Mai, Y. Chang, Y. You, L. He, T. Chen, *J. Controlled Release* **2021**, *331*, 270.
[3] A. C. Schmitz, D. Gianfelice, B. L. Daniel, W. P. T. M. Mali, M. A. A. J. van den Bosch, *Eur. Radiol.* **2008**, *18*, 1431.
[4] A. D. Kaye, M. W. Motejunas, L. A. Bonneval, K. P. Ehrhardt, D. R. Latimer, A. Trescot, K. E. Wilson, I. N. Ibrahim, E. M. Cornett, R. D. Urman, A. D. Kaye, M. W. Motejunas, L. A. Bonneval, K. P. Ehrhardt, D. R. Latimer, A. Trescot, K. E. Wilson, I. N. Ibrahim, E. M. Cornett, R. D. Urman, K. D. Candido, *Best Pract. Res., Clin. Anaesthesiol.* **2019**, *33*, 465.
[5] N. Y. Rapoport, A. M. Kennedy, J. E. Shea, C. L. Scaife, K. H. Nam, *J. Controlled Release* **2009**, *138*, 268.
[6] S. M. Chowdhury, T. Lee, J. K. Willmann, *Ultrasonography* **2017**, *36*, 171.
[7] M. Bok, Z. J. Zhao, S. Jeon, J. H. Jeong, E. Lim, *Sci. Rep.* **2020**, *10*, 2027.

© 2023 The Authors. Advanced Materials Technologies published by Wiley-VCH GmbH

2365709x, 2023, 16, Downloaded from https://onlinelibrary.wiley.com/doi/10.1002/admt.202202173 by South Korea National Provision, Wiley Online Library on [11/09/2023]. See the Terms and Conditions (https://onlinelibrary.wiley.com/terms-and-conditions) on Wiley Online Library for rules of use; OA articles are governed by the applicable Creative Commons License

[8] S. Subramaniam, J. Bober, J. Chao, S. Zehtabchi, *Acad. Emerg. Med.* **2016**, *23*, 1298.
[9] T. Hakozaki, H. Takiwaki, K. Miyamoto, Y. Sato, S. Arase, *Skin. Res. Technol.* **2006**, *12*, 105.
[10] T. J. Stephens, M. L. Sigler, P. D. Hino, A. le Moigne, L. Dispensa, *J. Clin. Aesthet. Dermatol.* **2016**, *9*, 25.
[11] J. R. Marin, A. J. Dean, W. B. Bilker, N. L. Panebianco, N. J. Brown, E. R. Alpern, *Acad. Emerg. Med.* **2013**, *20*, 545.
[12] H. C. Tsai, C. H. Tsai, W. S. Chen, C. Inserra, K. C. Wei, H. L. Liu, *Sci. Rep.* **2018**, *8*, 17720.
[13] L. Chen, I. Rivens, G. ter Haar, S. Riddler, C. R. Hill, J. P. M. Bensted, *Ultrasound Med. Biol.* **1993**, *19*, 67.
[14] D. H. Suh, J. H. Choi, S. J. Lee, K. H. Jeong, K. Y. Song, M. K. Shin, *J. Costmet Laser Ther.* **2015**, *17*, 230.
[15] J. H. Park, S. D. Lim, S. H. Oh, J. H. Lee, U. C. Yeo, *Skin Res. Technol.* **2017**, *23*, 384.
[16] M. Tanter, M. Pernot, J. F. Aubry, G. Montaldo, F. Marquet, M. Fink, *Int. J. Hyperthermia* **2007**, *23*, 141.
[17] J. Jang, J. H. Chang, *Sensors* **2016**, *16*, 1248.
[18] K. Harada, T. Azuma, T. Inoue, T. Takeo, S. Takagi, Y. Matsumoto, N. Sugita, M. Mitsuishi, in *Procedia CIRP*, Elsevier, New York **2013**, pp. 290–293.
[19] Z. Liang, J. Li, *Phys. Rev. Lett.* **2012**, *108*, 114301.
[20] Y. Li, G. Yu, B. Liang, X. Zou, G. Li, S. Cheng, J. Cheng, *Sci. Rep.* **2014**, *4*, 6830.
[21] Y. X. Shen, Y. G. Peng, F. Cai, K. Huang, D. G. Zhao, C. W. Qiu, H. Zheng, X. F. Zhu, *Nat. Commun.* **2019**, *10*, 3411.
[22] G. S. Kino, *Acoustic Waves: Devices, Imaging, and Analog Signal Processing*, Prentice-Hall, Englewood Cliffs, NJ **1987**.
[23] L. Bindi, P. J. Steinhardt, N. Yao, P. J. Lu, *Science* **2009**, *324*, 1306.
[24] J. G. Allpress, J. V. Sanders, *Surf. Sci.* **1967**, *7*, 1.
[25] S. Konijnenberg, A. J. L. Adam, H. P. Urbach, *Optics* **2021**.
[26] M. Bok, Y. Lee, D. Park, S. Shin, Z. J. Zhao, B. Hwang, S. H. Hwang, S. H. Jeon, J. Y. Jung, S. H. Park, M. Bok, Y. Lee, D. Park, S. Shin, Z.-J. Zhao, B. Hwang, S. H. Hwang, S. H. Jeon, J.-Y. Jung, S. H. Park, J. Nah, E. Lim, J.-H. Jeong, *Nanoscale* **2018**, *10*, 13502.
[27] M. Bok, Z. J. Zhao, S. H. Hwang, H. J. Kang, S. Jeon, J. Ko, J. Jeong, Y. S. Song, E. Lim, J. H. Jeong, *Pharmaceutics* **2020**, *12*, 954.
[28] Y. Jeong, J. Park, J. Lee, K. Kim, I. Park, *ACS Sens.* **2020**, *5*, 481.

© 2023 The Authors. Advanced Materials Technologies published by Wiley-VCH GmbH

2365709x, 2023, 16, Downloaded from https://onlinelibrary.wiley.com/doi/10.1002/admt.202202173 by South Korea National Provision, Wiley Online Library on [11/09/2023]. See the Terms and Conditions (https://onlinelibrary.wiley.com/terms-and-conditions) on Wiley Online Library for rules of use; OA articles are governed by the applicable Creative Commons License